NUMERICAL SIMULATION OF ROTATING STALL IN A TWO-STAGE AXIAL FAN

***Lei Zhang*[1,2,*]*, Abraham Engeda*[2]

[1] Department of Power Engineering, North China Electric Power University, 071003, Baoding, China

[2] Department of Mechanical Engineering, Michigan State University, 48823, East Lansing, United States

[*] Corresponding author; Email: zhang_lei@ncepu.edu.cn

Computational fluid dynamics calculations using high-performance parallel computing were conducted to simulate the prestall flow of a two-stage axial fan. The simulations were run with a full-annulus grid that models the 3D, viscous, unsteady blade row interaction without the need for an artificial inlet distortion to induce stall. The simulation shows the initiation and development of the stall inception in two rotors of the axial fan. The results show that the stall inception first occurs in the second stage. The spike-type stall inception occurred in the second stage, which is different from the common views. The starting positions of stall inception in both rotors are in the same circumferential direction, and the stall inceptions in both rotors turn into mature stall cells at the same time. Also, the rotation speed of the stall inception and rotating stall in the two rotors are the same. The rotating stall in the first and second stage rotor impellers are both directly induced by the blade tip leakage flow. However, the blocked flow in the second stage rotor strengthens the leakage flow in the blade tip of the first stage rotor indirectly, resulting in the formation of stall inception.

Key words*: axial fan, rotating stall, stall inception,numerical simulation.*

1. Introduction

Axial fan is one of the important accessory equipment in biomass power plant. It commonly displays two kinds of unsteady flow phenomena such as surge and rotating stall when they operate at flow rates substantially below the design point. These instabilities can cause noise and strong dynamical loading on the blades. Therefore, they cannot be tolerated during fan operation and result in a narrower operation range. Many efforts have been concentrated on the mechanism of stall inception and the controlling methods to avoid or delay the occurrence of rotating stall in turbo machinery [1].

The study of stall inception is not only an important part of rotating stall research, but the basis of stall control. There are two kinds of widely accepted inception, namely the modal wave type inception and spike type inception proposed by Camp and Day [2]. According to their research, the modal wave type inception rotates at less than 50% rotor speed. It represents a large scale wave with small amplitude. On the contrary, the spike type inception mostly occurs in the tip region of blades with a rotating speed of 60% to 80% rotor speed, and it represents a small scale wave with large amplitude. The modal wave type inception was first captured in a single-stage, axial compressor with high pressure ratio by Mcdougall[3]. Then the modal wave type inception was found by Garnier[4],

which verified the previous theories[2]. The spike type inception was first found and researched by Day[5]. Afterwards, the structure, characteristics and development law were investigated by many researchers with experiments and numerical simulations [6-7].

The impact factors on the type of stall inception have always been a controversial area. In recent years, it is certain that the generation mechanism and form of the stall inception are influenced by the design parameters and operation parameters of the machine. Lots of studies on the influence of design parameters such as hub ratio, tip clearance and blade row spacing have been undertaken [8-9]. Based on a new kind of detection technology, Cameron studied the relationship between stall inception and tip clearance in a high speed axial compressor [10]. The influence of blade row spacing on the starting position of stall is verified by Zhu through experiments. It was found that this is vital to the number of stall cells that form [11]. On the other hand, rotating speed and the marching of rotor and stator are important to stall inception as well. Through studying the stall inception under different rotating speeds on the same fan, Choi found the stall inception to be quite sensitive to the rotating speed [12].

During the past 20 years, studies on stall through unsteady simulations in turbomachinery have achieved valuable findings of the flow structure leading to stall [13-14]. However, they were focused on the single stage turbomachinery. In fact, many multi-stage turbomachinery are used in industry, and the instability process in multi-stage machines is more complex. Knapke conducted a numerical investigation on rotating stall in a two-stage counter-rotating compressor [15]. Peng investigated the effects of variable stator vanes on the occurrence of rotating stall in an axial multi-stage-compressor using an in-house CFD based aeroelastic code [16].

The intent of this work is to use the numerical method to capture the inherent behaviour of a two-stage axial fan as it is throttled into stall. This paper is organized as follows. First, the numerical methods are introduced, such as the establishment of the geometric model, meshing strategy, and distribution of numerical probes. Second, grid independence verifications are conducted to provide assessment of the meshing quality, steady simulation results, and experimental results are compared to show evidence that the computational model are reasonable. Third, the unsteady phenomenon of rotating stall is simulated with the throttle valve model. Fourth, the unsteady flow field during the occurrence and development of stall inception in the two stages are analyzed. Finally, the induction mechanism of the spike type stall inception in the second rotor is discussed.

2. Numerical Simulation

2.1Geometric Model and Meshing

The geometric model of the axial fan is established as shown in Figure 1. There are six main parts of the fan, namely the inlet collector, the first rotor, the first stator, the second rotor, the second stator and the outlet diffuser. The structure parameters are listed in Table 1.The first and second rotors are marked as Rotor 1 and Rotor 2, and the stators are marked as Stator 1 and Stator 2, respectively. ICEM CFD software is used to generate the multi-block structures grids of the whole axial fan. Near the leading-edge and trailing-edge of each blade, the separation of the

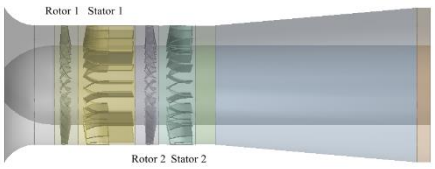

Figure 1: Geometric Model of Axial

Table 1: Structure Parameters of

Structure parameters	values
Number of rotor blade	24
Number of stator blade	23
Hub ratio	0.668
Blade height (m)	0.29
Rotating speed (r/min)	1490

boundary layer will form separation vortexes, the grids of those parts are refined, as well as the tip clearance grids, to improve the calculation accuracy. Figure 2(a) shows the grids around the leading-edge and trailing-edge. Furthermore, the sliding grid model is adopted at the interface between the rotor and the stator. In addition, the boundary layer grids are used on the surfaces of blades to ensure that the mean normalized wall distance, y+, is smaller than 5. Figure 2(b) shows the local grid of the rotor blade and the enlarged view around the impeller.

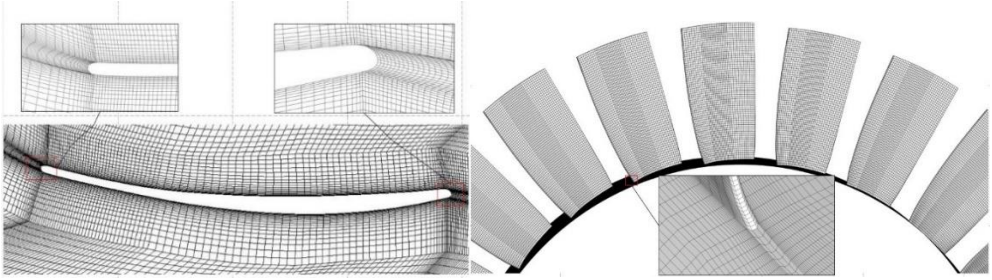

(a) (b)

Figure 2: (a)Computational Grid Around Main Blade Edge; (b)Local Grid of the Rotor Blade and Enlarged View Around the Impeller

2.2 Distribution of Numerical Probes

In order to monitor the relative velocity and pressure transients in the corresponding positions before and after the occurrence of rotating stall, 12 and 6 numerical probes are set circumferentially in the first and second rotors, respectively. As shown in Figure 3, the six numerical probes in the first rotor labeled as l1, l2, l3, m1, m2 and m3, are set inside the 3 passages of which the interval is 30 °, and the other 6 probes are set at the inlet of the 3 passages. The probes in each passage are at 50% and 90% blade height. The 6 numerical probes in the second rotors, labeled as l7, l8, l9, m7, m8, and m9, are distributed in the corresponding passages according to placement in the first rotor.

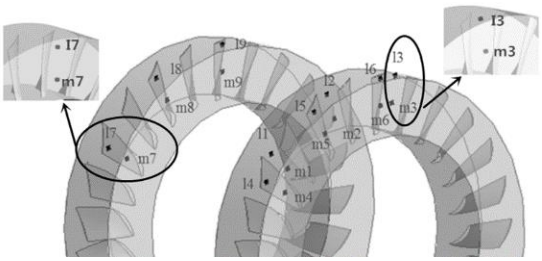

Figure 3: Distribution of the Numerical Probes in Two Rotors

2.3 Methods of Numerical Calculation

As for the numerical simulation, the collector inlet and diffuser outlet are selected as the inlet and outlet of the calculation regions. The pressure inlet and pressure outlet boundary condition are adopted respectively. Moving reference frame (MRF) is selected for the rotating region of the two rotors with a rotating speed of 1490 r/min. The domains of the fan are connected to each other with the interface boundary condition, and the wall boundary condition is applied to all the other parts of the fan. A 3D unsteady Reynolds time-averaged Navier-Stokes equation is selected as the control equation for the simulation, and SST model, which is more suitable for rotating flow and flow separation, is adopted as the turbulence model. Discrete control equations of the finite volume method are used, wherein a second-order upwind difference scheme and a central difference scheme are adopted to discretize convection and diffusion terms, respectively.

To realize numerical stall, the throttle valve model is used in this paper. The operating condition of the ventilation system is determined by the intersection of the fan performance curve and valve throttling line, which is directly connected in structure. The operating point changes with the throttle opening and the slope of performance curve and throttle line differs at the same operating point, thus the stability analysis can be conducted. The throttle function can be expressed as follows[17]:

$$Ps_{out}(t) = Pi_{in} + \frac{1}{2}\frac{k_0}{k_1}\rho U^2 \tag{1}$$

Where Ps_{out} and Pi_{in} represent the outlet back pressure and environmental pressure, k_0 and k_1 are constant and valve opening respectively. ρ represents the air density, and U is the axial velocity at the outlet.

3. Results and Discussions

3.1 Grid Independence Verification and Steady Simulation

The grid independence verification is conducted in this paper in order to minimize the influence of grid number on the simulation results. Geometric models with grid numbers of 2250000, 4170000, 5300000 and 6420000 were selected, and the steady simulation results under different grid number are compared with the experimental results as shown in Figure 4. It can be seen that the impact of gird number on the simulation results can be neglected when it comes to 5300000. Also, the trend of the total pressure performance curve obtained through steady simulation is consistent with that of the sample curve, and the relative error of total pressure is within the range of 1.523% to 5.245%, which indicates that the fan model established can be used for simulation. To better compare the numerical and experimental results, the boundary conditions in the grid independence calculations are velocity at the inlet and outflow at the outlet. The inlet velocities are obtained from experimental results.

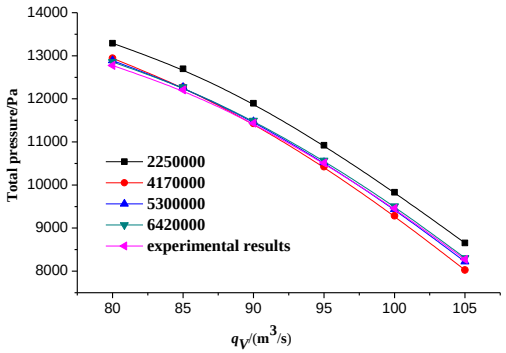

Figure 4: Relation between Total Pressure and Volume Flow Rate

3.2 Unsteady Simulation of Rotating Stall

The relationship between total pressure and flow rate obtained from steady and unsteady simulations is illustrated in Figure 5. The curve shows the total pressure fluctuation under steady simulation when the flow rate is below 73m^3/s. The convergence with the flow of 73m^3/s is taken as the initial condition for unsteady simulation, and the convergent results can be obtained under certain outlet back pressure. Then the valve opening k_1 is set to 1, and the outlet pressure can be indirectly improved by continuously decreasing throttle valve opening until the occurrence of rotating stall in the fan. Three operating conditions of k_1=0.7, k_1=0.66 and k_1=0.658 are listed on the left of the flow rate of 73m^3/s. It can be seen that the total pressure of the fan decreases gradually along with the decrease of the throttle valve, and it reaches its minimum when k_1=0.658. Afterwards, the total pressure does not remain stable and fluctuations become larger with the decrease of throttle valve. When it comes to

k_1 =0.657, a steep drop of both the total pressure and flow occurs, which indicates that the fan experiences rotating stall.

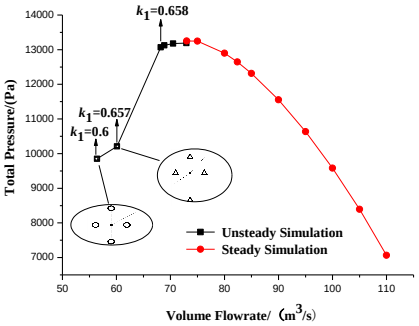

Figure 5: Total Pressure vs. Volume Flowrate

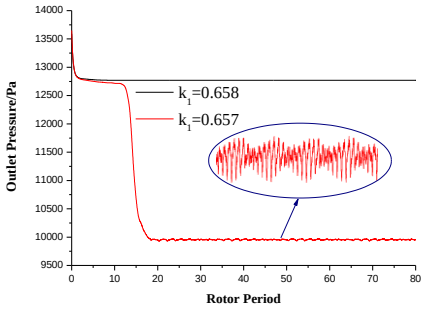

Figure 6: Curves of the Outlet Pressure with time

Figure 6 illustrates the occurrence of rotating stall with the comparison of fan outlet pressure when the throttle valve is 0.658 and 0.657. While k_1 is 0.658, the outlet pressure maintains stability and the fan is still in the state of stable operation. However, the outlet pressure experiences a steep drop after several rotor cycles and fluctuations show a sine wave trend with a large magnitude when k_1 is 0.657. The whole process of the outlet pressure changes indicates the occurrence and development of rotating stall.

3.3 Confirmation of the Occurrence Position of Stall Inception

In two-stage axial fan, the confirmation of the stage where stall inception occurs is important, and the research of the development process of stall inception helps to shed light on the mechanism of rotating stall. It can be determined by monitoring the relative velocity of the flow in the rotor passages to confirm the occurrence of the stall inception in rotors. The relative velocity from the m4 and m7 numerical probes for k_1 0.657 is shown in Figure 7. The relative velocity value of monitoring point m7 is moved up 40 units for comparison. As shown in Figure 7, both rotors experience the phenomenon of stall inception to stall cell formation. However, the relative velocity of m7 experiences large fluctuations in amplitude at the 13th rotor cycle while that of m4 remains stable. It can be concluded that the unsteady fluctuations with large amplitudes first occur in the second rotor.

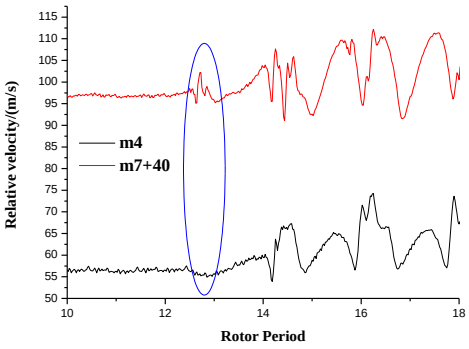

Figure 7: Curves of Relative Velocity with time at m4 and m7 for k_1 =0.657

The relative velocities of the two rotors in the corresponding passages when k_1 is 0.657 are shown in Figure 8. The relative velocity value of monitoring point m5 ,and m8 are moved up 30 units and the relative velocity value of monitoring point m6 ,and m9 are moved up 60 units, for comparison. In Figure 8(a), it can be seen that the slopes of the two lines are different. The rotating speeds at the two different moments are 0.67 and 0.5 , where represents the rotating speed of the stall inception and stall cell. Similarly, the rotating speed corresponding lines 3 and 4 in Figure 8(b) are 0.67 and 0.5 . According to the basic characteristics of modal type and spike type stall inception, it

can be shown that the unsteady fluctuations occurring in the two rotors are both spike type stall inception. The slope of line1 and line 3 are consistent with the occurrence of stall inception in both rotors. It can be seen that spike type stall inception first occurs in the second rotor, and the rotating speed of stall inception in both rotors is the same. After the formation of a stall cell, the stall cells in both rotor impellers share the same rotating speed. Usually in low and intermediate pressure compressors, spike stall inception is seen in the first rotor. However, the spike in downstream blade row occurs in the two-stage axial fan, which agrees with Camp[26].

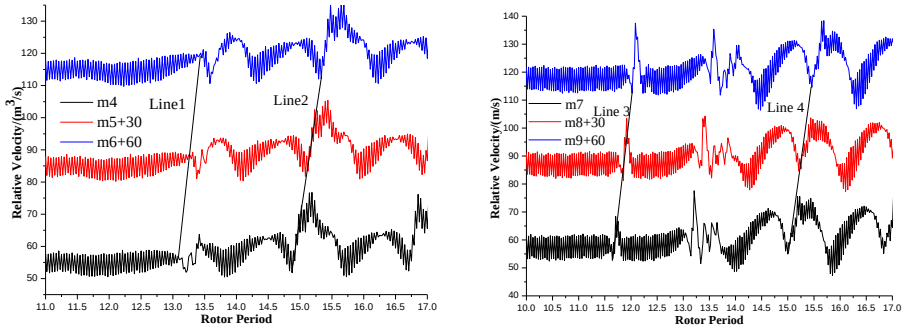

(a) (b)

Figure 8: Evolution of Relative Velocity with Different Probes for k_1 =0.657; (a) Evolution of Relative Velocity at Points of m4, m5 and m6 in Rotor 1, (b) Evolution of Relative Velocity at Points of m7, m8 and m9 in Rotor 2

In order to identify the precise starting point of stall inception in both rotors, the relative velocity in the passages of the two rotors obtained by numerical probes undergoes differential analysis. Figure 9(a) illustrates the difference between the relative velocity of m4 and m6. It can be seen that stall inception occurs at point A (12.95T) in the first rotor. After about 2 rotor cycles, the stall inception develops into a stall cell at point B (14.5T). While in the second rotor, as shown in Figure 9(b), stall inception occurs at point C (11.75T), and after approximately 2.5 rotor cycles, a stall cell comes into being at point E (14.5T). However, it cannot be ignored that the fluctuations become enhanced from point D (12.95T). Hence, spike type stall inception first occurs at 11.75T in the second rotor while the first rotor remains stable which is consistent with the conclusion above. After 1.2T, the same phenomenon occurs in the first rotor. Finally the two rotors enter rotating stall at 14.5T synchronously. Comparing Figure 9 with Figure 8, it can be further concluded that rotating stall derives from the unsteady fluctuation in the second rotor. Through a short period of development, the occurrence of stall inception in the first rotor influences that of the second rotor impeller. This accelerates the process of stall inception in the second impeller. Due to the interaction between the two rotors, the disturbance in both rotor turns into a mature stall cell at the same time. To show this requires flow field analysis during the occurrence and development of stall in both rotors.

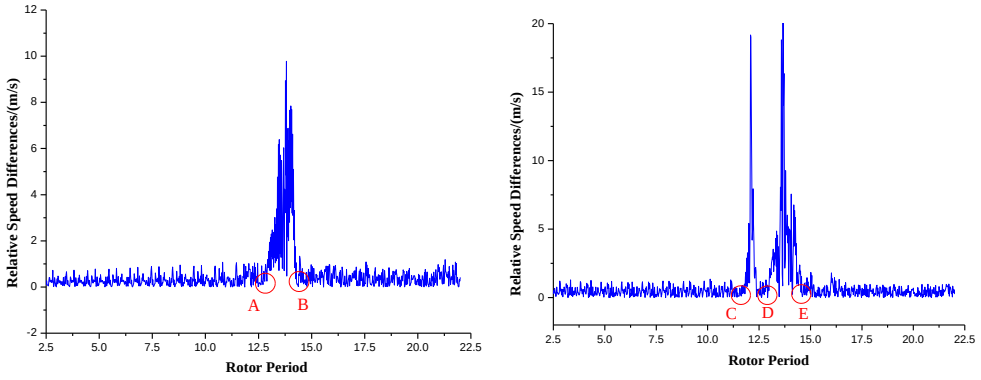

(a) (b)

Figure 9: Difference Curves of Relative Velocity in the Passages of the First and Second Rotors; a) Differences of Relative Velocity at Points of m4 and m6 b) Differences of Relative Velocity at Points of m7 and m9

3.4 Flow Field Analysis during the Occurrence and Development of Stall Inception

Three typical times, 12T, 13T and 14T, are selected for k_1 = 0.657 to give a thorough analysis of stall development in the view of the flow field. As shown in Figure 10, the stream line distribution of the passages in both rotors at the 95% blade height is investigated. It can be clearly seen in Figure 10(a) that a separation vortex occurs in four continuous passages of the second rotor while the flow field in the first rotor remains uniformly distributed. In Figure 10(b), drastic flow separation occurs in the blade tip area of multiple convective passages in both rotors, which indicates the beginning of stall inception in both impellers. By comparing the flow field in both rotors, it is obvious that the passages in the first and second rotors correspond to each other, and the starting position of stall in both rotors is the same in the circumferential directions of the fan. According to this observation the stall inception is likely influenced and induced by flow separation in the corresponding passages of the second rotor.

On the other hand, before the occurrence of stall inception in the first rotor, the development of stall inception in the second rotor seems to be quite slow, and the number of passages influenced by the separation vortex and back flow does not increase greatly. When it comes to the 14T, as shown in Figure 10(c), not only does the number of passages occupied by the separation vortex in the second rotor greatly increase, but the intensity of the separation vortex and back flow is enhanced in each passage compare to that in the 13T. Therefore, it can be concluded that once stall inception occurs in the first rotor, stall inception in the second rotor is influenced as well. The interaction between the two rotors results in the rapid aggravation of stall inception in both rotors, and stall cells are generated soon after. This provides solid evidence for the deduction above and describes the development process of stall inception in both rotors.

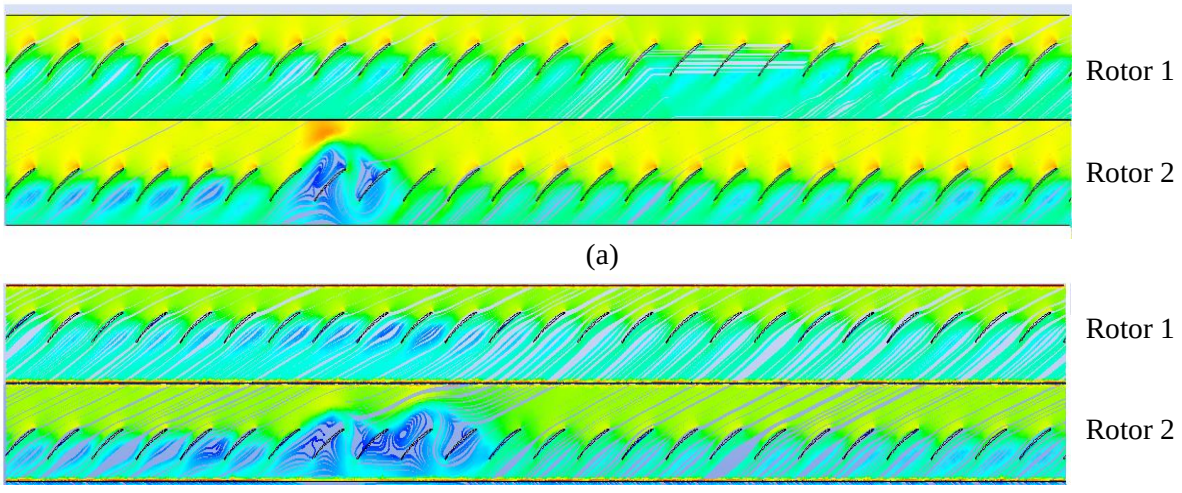

(b)

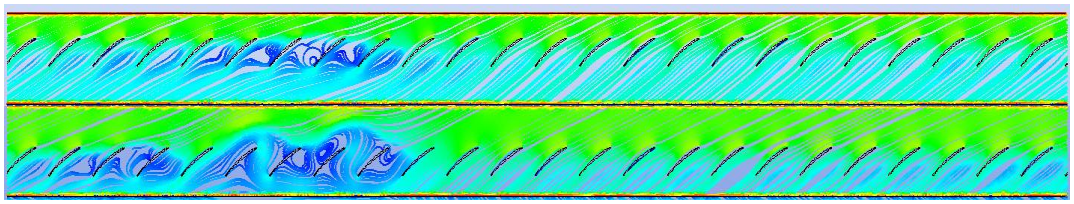

(c)

Figure 10: Stream Line Distribution of the Passages in Both Rotors at the 95% Blade Height; The12th Rotor Period; The 13th Rotor Period; The 14th Rotor Period

3.5 The Mechanism of Stall Inception in the Second Rotor

The contours of the static pressure on the blade pressure side and suction side in the second rotor near stall are shown in Figure 11. It can be seen that the static pressure of the pressure side is much higher than that of the suction side, which is the essential condition for the occurrence of the tip clearance flow. At the leading edge of the blade tip area, a low pressure region exists on the suction side of blade. The large pressure difference makes it likely that the tip clearance flow will occur at the leading edge of the blade. Combining this result with the separation vortex in Figure 10, it can be shown that the tip clearance flow mainly occurs at the leading edge of the suction side of blades before stall. With the development of the tip clearance flow along the axial direction, the separation vortex, which is mixed with the mainstream, moves away from the suction side of the blades gradually. Therefore the low pressure area also disappears at the trailing edge of blades.

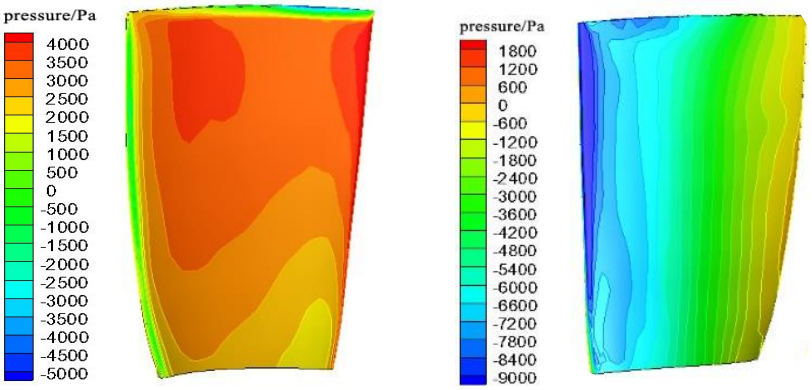

(a) (b)

Figure 11: Contours of the Static Pressure of Blade near Stall Condition; (a) Pressure Side;(b) Suction Side

As shown in Figure 12, the distributions of static pressure and stream lines at 95% blade height in four convective passages of the second rotor are illustrated. It can be concluded that the flow field is highly impacted by the tip clearance flow. Due to the different directions of the tip clearance and mainstream flows, interaction and mixing of both flows leads to the low speed flow occupying a large number of the passages.

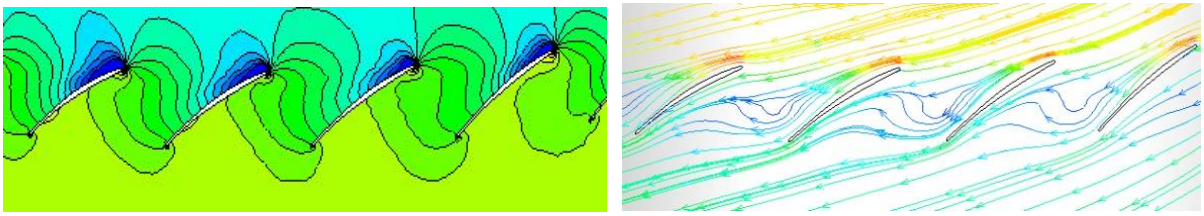

(a) (b)

Figure 12: Contours of the Static Pressure and Distribution of Stream Line near Stall Condition at the 95% Blade Height in the Second Rotor; (a) Contours of Static Pressure (b) Distributions of Stream Lines

Based on the analysis above, the influence of the blade tip clearance flow mainly comes from the mixing and interaction between the tip clearance and mainstream. The tip clearance flow (W_{jet}) comes from the pressure side of the blades and the mainstream flow (W_p) comes from the passage inlet form into independent vortex eventually. The stream line twined around the vortex forms a spatial structure, leading to the low speed area. Due to the curling effect of tip clearance, the axial backflow phenomenon may occur near the blade tip. The development schematic diagram of the tip clearance flow is shown in Figure 13.

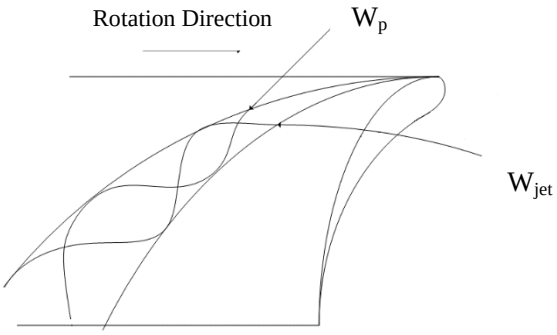

Figure 13: Schematic Diagram of the Tip Clearance Flow

4. Conclusions

In this paper, rotating stall in a two-stage variable pitch axial fan is numerically studied, and the association analysis on the generation of stall inception in different stages was conducted. Also, the induced mechanism of stall inception is discussed. The conclusions can be drawn as follows:

(1) Stall inception begins in the second rotor with spike type inception, and the overall characteristics have a positive gradient at stall, which is different from Day[2] and the same as Camp[18]. The rotating speed of stall inception in both rotors and the inception type are the same. After the formation of the stall cell, both stall cells share the same rotating speed.

(2) Stall inception in the first rotor is induced by that of the second rotor since they share the same position in the circumferential direction. The occurrence of stall inception in the first rotor accelerates the development of stall inception in the second rotor. Due to the interaction between the two rotors, a mature stall cell develops at the same time in both rotors.

(3) The development of the stall inception in the second rotor is induced by the tip clearance flow near the leading edge of blades. The mixing and interaction between the tip clearance flow and mainstream flow lead to a separation vortex and backflow.

Acknowledgment: This research was supported by National Natural Science Foundation of China(Grant No.11602085), and Natural Science Foundation of Hebei Province, China (Grant No. E2016502098).

REFERENCES

[1] Gao, L., Li, R., Miao, F., Cai, Y., Unsteady Investigation on Tip Flow Field and Rotating Stall in Counter-Rotating Axial Compressor, *Journal of Engineering for Gas Turbines and Power*, 2015, 137(7): 072603.

[2] Camp, T.R., Day, I.J., A study of spike and modal stall phenomena in a low-speed axial compressor, *Journal of Turbomachinery.*, 1998, 120(3): 393-401.

[3] McDougall, N.M., Cumpsty, N.A., Hynes, T.P., Stall inception in axial compressors, *Journal of Turbomachinery.*, 1990, 112: 116-125.

[4] Garnier, V.H., Epstein A.H., Greitzer, E.M., Rotating waves as a stall inception indication in axial compressors, *Journal of mechanical design*., 1991, 113(2): 290-302.

[5] Day, I.J., Stall inception in axial flow compressors, *Journal of turbomachinery*,, 1993, 115(1): 1-9.

[6] Kazutoyo, Y., Hiroaki, K., Ken-ichiro, I., Masato, F., An Explanation for Flow Features of Spike-Type Stall Inception in an Axial Compressor Rotor, *Journal of Turbomachinery*., 2013, 135(2): 021023.

[7] Andreas, L., Gunther, B., Numerical Simulation and Evaluation of Velocity Fluctuations during Rotating Stall of a Centrifugal Pump, *Journal of Fluids Engineering.*, 2011, 133(8):205-216.

[8] Gourdain, N., Burguburu, S., Leboeuf, F., Simulation of rotating stall in a whole stage of an axial compressor, *Computers & Fluids.*, 2010, 39: 1644-1655.

[9] Inoue, M., Kuroumaru, M., Yoshida, S., Short and long length-scale disturbances leading to rotating stall in an axial compressor stage with different stator/rotor gaps, *Journal of turbomachinery*., 2002, 124(3): 376-384.

[10] Cameron, J.D., Bennington, M.A., Ross, M.H., The Influence of Tip Clearance Momentum Flux on Stall Inception in a High-Speed Axial Compressor, *Journal of Turbomachinery.*, 2013, 135(5): 1-11.

[11] Zhu, J.Q., Liu, Z.W., Ma, C.B., Influence on Stalled Flow Field of Gap between Rotor and Stator, *Journal of Northwestern Polytechnical University.*, 1993, 3: 001.[in Chinese]

[12] Choi, M., Vahdati, M., Effects of Fan Speed on Rotating Stall Inception and Tecovery, *Journal of Turbomachinery.*, 2011, 133(4): 1-8.

[13] Cornelius, C., Biesinger, T., Galpin, P., Braune, A., Experimental and Computational Analysis of a Multistage Axial Compressor Including Stall Prediction by Steady and Transient CFD Methods, *Journal of Turbomachinery.*, 2014, 136(6): 061013.

[14] Gao, L.M., Li, X.J., Xie, J., Prediction of onset of rotating stall using small perturbation theory for contra-rotating compressors, *Acta Aeronautica et Astronautica Sinica.*, 2013, 34(3): 533-540.

[15] Knapke, R.D., Turner, M.G., List, M.G., Galbraith, D.S., Beach. T., Merchant. A.A., Time accurate simulations of a counter-rotating aspirated compressor, *ASME Turbo Expo 2008*: Power for Land, Sea, and Air. American Society of Mechanical Engineers, 2008: 481-496.

[16] Peng, C., Numerical predictions of rotating stall in an axial multi-stage-compressor, *ASME Turbo Expo 2011*: GT2011-45503.

[17] Gourdain, N., Burguburu, S., Leboeuf, F., & Michon, G. J. Simulation of rotating stall in a whole stage of an axial compressor. *Computers & Fluids*, 2010, *39*(9), 1644-1655.

[18] Camp, T.R., Aspects of the off-design performance of axial flow compressors, Ph.D.thesis, Department of Engineering, University of Cambridge 1995.